JACS
JOURNAL OF THE AMERICAN CHEMICAL SOCIETY

ARTICLE

pubs.acs.org/JACS

# Mechanistic Insights for Block Copolymer Morphologies: How Do Worms Form Vesicles?

Adam Blanazs,[†] Jeppe Madsen,[†] Giuseppe Battaglia,[‡] Anthony J. Ryan,[†] and Steven P. Armes*[,†]

[†]Department of Chemistry, The University of Sheffield, Brook Hill, Sheffield S3 7HF, United Kingdom

[‡]Department of Biomedical Science, The University of Sheffield, Western Bank, Sheffield S10 2TN, United Kingdom

Supporting Information

**ABSTRACT:** Amphiphilic diblock copolymers composed of two covalently linked, chemically distinct chains can be considered to be biological mimics of cell membrane-forming lipid molecules, but with typically more than an order of magnitude increase in molecular weight. These macromolecular amphiphiles are known to form a wide range of nanostructures (spheres, worms, vesicles, etc.) in solvents that are selective for one of the blocks. However, such self-assembly is usually limited to dilute copolymer solutions (<1%), which is a significant disadvantage for potential commercial applications such as drug delivery and coatings. In principle, this problem can be circumvented by polymerization-induced block copolymer self-assembly. Here we detail the synthesis and subsequent in situ self-assembly of amphiphilic AB diblock copolymers in a one pot concentrated aqueous dispersion polymerization formulation. We show that spherical micelles, wormlike micelles, and vesicles can be predictably and efficiently obtained (within 2 h of polymerization, >99% monomer conversion) at relatively high solids in purely aqueous solution. Furthermore, careful monitoring of the in situ polymerization by transmission electron microscopy reveals various novel intermediate structures (including branched worms, partially coalesced worms, nascent bilayers, "octopi", "jellyfish", and finally pure vesicles) that provide important mechanistic insights regarding the evolution of the particle morphology during the sphere-to-worm and worm-to-vesicle transitions. This environmentally benign approach (which involves no toxic solvents, is conducted at relatively high solids, and requires no additional processing) is readily amenable to industrial scale-up, since it is based on commercially available starting materials.

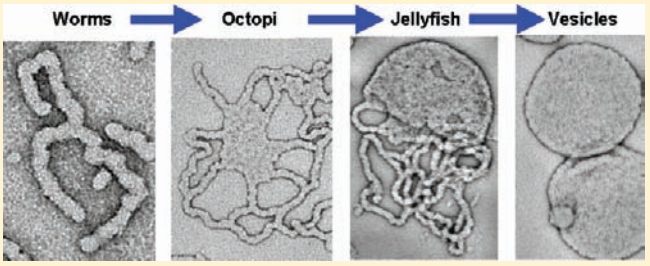


## INTRODUCTION

The aqueous self-assembly of amphiphilic lipids to form cell membranes is essential for the existence of life, as it is a prerequisite for cellular compartmentalization, gene segregation, and the generation of chemical gradients.[1] Small molecule surfactant self-assembly in aqueous solution has been extensively studied for many decades.[2,3] It is well-known that the surfactant concentration and its hydrophilic/hydrophobic balance dictate the precise nature of the various nanostructures formed in aqueous solution (i.e., spherical micelles, wormlike micelles, or vesicles).[2−4]

Controlled polymerization techniques (such as ionic and "living" radical polymerization) have enabled the synthesis of a wide range of amphiphilic block copolymers that can self-assemble to form spherical micelles,[5] wormlike micelles,[6−9] toroids,[10] micellar networks,[11] and vesicles (aka polymersomes)[5,12−15] for various applications.[16] Compared to surfactant micelles, block copolymer aggregates are much more robust: the exchange kinetics of individual chains between aggregates is typically significantly slower, leading in many cases to nonergodic (i.e., kinetically frozen) systems.[17,18] Moreover, higher molecular weights and chain entanglements lead to thicker, more resilient vesicular membranes compared to lipid counterparts.[19−21] In particular, copolymer vesicles that can respond to external stimuli such as pH,[22,23] oxidation,[24] and temperature[25] offer considerable potential for intracellular drug delivery.[16,26] However, in many cases, the processing route (e.g., solvent exchange, film rehydration, pH switch, etc.) used to produce block copolymer aggregates can influence their final morphology to a similar extent as the hydrophobic/hydrophilic balance of the copolymer.[27] Furthermore, such processing techniques are normally limited to dilute copolymer solutions (<1%), which is a significant disadvantage for commercial viability.

Polymerization-induced self-assembly is well established in the bulk for toughened thermosets and elastomers formed by step polymerization.[28,29] However, as far as we are aware, there are very few reports[30−32] of polymerization-induced self-assembly by living radical polymerization under aqueous dispersion polymerization conditions. This is not particularly surprising: most water-miscible monomers do not form water-insoluble polymers, which is an essential prerequisite for such formulations. Recently, we reported the reversible addition−fragmentation chain transfer

**Received:** July 7, 2011
**Published:** August 17, 2011

(RAFT) aqueous dispersion polymerization of 2-hydroxypropyl methacrylate (HPMA) using a water-soluble poly(glycerol monomethacrylate) (PGMA) chain transfer agent (CTA).[33] Importantly for this formulation, HPMA monomer is water-miscible up to 13 w/v % at room temperature, yet forms a water-insoluble polymer. In the present work, we further investigate this formulation. We show that spherical micelles, wormlike micelles, and vesicles are *predictably* obtained for HPMA polymerizations conducted at 10 w/v %. Complete monomer conversions are achieved at 70 °C within 2 h, and the particles comprise near-monodisperse copolymer chains. Furthermore, careful monitoring of the in situ polymerization by transmission electron microscopy (TEM) reveals various intermediate structures (including branched worms, partially coalesced worms, nascent bilayers, "octopi", "jellyfish", and finally pure vesicles) that provide important mechanistic insights regarding the evolution of the particle morphology.

## MATERIALS AND METHODS

**Materials.** Glycerol monomethacrylate (GMA; 99.8%) was donated by Cognis Performance Chemicals (Hythe, U.K.) and used without further purification. 2-Hydroxypropyl methacrylate (HPMA) was donated by Cognis Performance Chemicals and was also purchased from Sigma Aldrich; in each case, monomer was passed through a DHR-4 inhibitor removal column (Scientific Polymer Products, Ontario, NY) prior to use. 2-Cyano-2-propyl dithiobenzoate (CPDB), 4,4′-azobis(4-cyanopentanoic acid) (ACVA; V-501; 99%) $D_2O$, anhydrous ethanol (99%), methacrylic anhydride (94%), *N*,*N*-dimethylaminopyridine (99%), and dialysis tubing (1 kD molecular weight cutoff) were purchased from Sigma Aldrich U.K. and were used as received. In the case of the CPDB, the manufacturer's stated purity was 97%, but $^1$H NMR analysis indicated a purity of only 75%. This reduced purity was taken in account when calculating the target degree of polymerization for the PGMA block. The water-soluble internal standard used in the NMR experiments, sodium 2,2 dimethyl-2-silapentane-5-sulfonate (DSS), and $CD_3OD$ were purchased from Goss Scientific (Nantwich, U.K.). Triethylamine, magnesium sulfate, sodium hydrogen carbonate, and sodium chloride were of Laboratory Reagent grade and purchased from Fisher Scientific (Loughborough, U.K.). All solvents were of HPLC quality and purchased from Fisher Scientific (Loughborough, U.K.).

**Synthesis of the $PGMA_{47}$ Macro-CTA.** CPDB RAFT agent (1.5 mmol, 0.33 g, purchased from Sigma Aldrich with 75% purity as judged by $^1$H NMR spectroscopy) and GMA monomer (89.6 mmol, 14.35 g) were weighed into a 50 mL round-bottomed flask and purged under $N_2$ for 20 min. ACVA (0.30 mmol, 83.7 mg, CTA/ACVA molar ratio = 5:1) and anhydrous ethanol (40 w/v %), which had been purged with $N_2$ for 30 min, were then added, and the resulting red solution was purged for a further 10 min. The sealed flask was immersed into an oil bath set at 70 °C for 80 min (GMA conversion 57%, see Supporting Information Figure S1) and quenched in liquid nitrogen. Methanol (50 mL) was added to the reaction solution, followed by precipitation into a 10-fold excess of cyclohexane (1 L). The precipitated PGMA macro-CTA was washed three times with cyclohexane and then dialyzed against methanol overnight (with three changes of methanol) using semipermeable cellulose tubing (SPECTRA/POR, corresponding to a molecular weight cutoff of 1000). $^1$H NMR indicated a degree of polymerization of 47 for the PGMA macro-CTA. $M_n$ = 14,100 and $M_w/M_n$ = 1.13, as judged by GPC using DMF eluent, a refractive index detector, and a series of near-monodisperse poly(methyl methacrylate) calibration standards.

**RAFT Aqueous Dispersion Polymerization of $PGMA_{47}$-$PHPMA_{160}$.** A typical protocol for the synthesis of $PGMA_{47}$-$PHPMA_{160}$ is as follows: $PGMA_{47}$ macro-CTA (0.150 g, 0.019 mmol) and HPMA monomer (0.4462 g, 3.1 mmol, Aldrich) were weighed into a 25 mL round-bottomed flask and purged with $N_2$ for 20 min. ACVA was added (1.8 mg, 0.0063 mmol, CTA/ACVA molar ratio = 3:1) and purged with $N_2$ for a further 5 min. Deionized water (5.4 mL, 10 w/v %), which had been purged with $N_2$ for 30 min, was then added, and the solution was degassed for a further 5 min prior to immersion in an oil bath set at 70 °C. The reaction solution was stirred overnight (16 h) to ensure complete HPMA monomer conversion and quenched with exposure to air.

**Kinetics of the Aqueous Dispersion Polymerization of HPMA for the *Sphere-to-Worm-to-Vesicle* Transitions When Targeting $PGMA_{47}$-$PHPMA_{200}$.** $PGMA_{47}$ macro-CTA (0.200 g, 0.026 mmol), HPMA monomer (0.7437 g, 5.2 mmol, Aldrich), and sodium 2,2-dimethyl-2-silapentane-5-sulfonate (DSS) (0.0225 g, 0.10 mmol, HPMA/DSS molar ratio = 50:1) were weighed into a 25 mL round-bottomed flask and purged with $N_2$ for 20 min. ACVA was added (1.2 mg, 0.004 mmol, CTA/ACVA molar ratio = 6:1) and purged with $N_2$ for a further 5 min. Deionized water (8.5 mL, 10 w/v %), which had been purged with $N_2$ for 30 min, was then added, a sample was immediately taken for $^1$H NMR analysis, and the solution was degassed for a further 5 min prior to immersion in an oil bath set at 70 °C. The "zero time" ($t$ = 0 min) for this polymerization was arbitrarily taken to be the point when the degassed reaction solution was first immersed in an oil bath set at 70 °C, rather than the time taken for the reaction solution to attain this temperature. Aliquots were then removed via syringe at various time intervals for $^1$H NMR and TEM analysis. $^1$H NMR samples were quenched by dilution in $D_2O$ at 20 °C. Monomer conversions were normalized using the DSS as an internal standard, and are expressed relative to the ratio of monomer to DSS observed at "zero time". For TEM analysis, aliquots were diluted 50-fold with water at 20 °C to generate 0.20 wt % dispersions.

**Polymer Characterization.** *$^1$H NMR Spectroscopy.* All NMR spectra were recorded on a 400 MHz Bruker Avance-400 spectrometer (64 scans averaged per spectrum).

*Gel Permeation Chromatography (GPC).* Copolymer molecular weights and polydispersities were determined using a DMF GPC setup operating at 60 °C and comprising two Polymer Laboratories PL gel 5 $\mu$m Mixed C columns connected in series to a Varian 390 LC multidetector suite (refractive index detector) and a Varian 290 LC pump injection module. The GPC eluent was HPLC grade DMF containing 10 mM LiBr at a flow rate of 1.0 mL min$^{-1}$. Dimethyl sulfoxide (DMSO) was used as a flow-rate marker. Calibration was conducted using a series of 10 near-monodisperse poly(methyl methacrylate) standards ($M_n$ = 625−618 000 g mol$^{-1}$). The chromatograms were analyzed using Varian Cirrus GPC software (version 3.3).

*Dynamic Light Scattering.* Intensity-average hydrodynamic diameters of the dispersions were obtained by DLS using a Malvern Zetasizer NanoZS instrument. Aqueous dispersions of 0.20 w/v % were analyzed using disposable cuvettes, and all data were averaged over three consecutive runs.

*Transmission Electron Microscopy (TEM).* Aggregate solutions were diluted 50-fold at 20 °C to generate 0.20 w/v % dispersions. Copper/palladium TEM grids (Agar Scientific) were surface-coated in-house to yield a thin film of amorphous carbon. The grids were then plasma glow-discharged for 30 s to create a hydrophilic surface. Individual samples (0.20 w/v %, 12 $\mu$L) were adsorbed onto the freshly glow-discharged grids for 1 min and then blotted with filter paper to remove excess solution. To stain the aggregates, uranyl formate (0.75 w/v %) solution (9 $\mu$L) was soaked on the sample-loaded grid for 20 s and then carefully blotted to remove excess stain. The grids were then dried using a vacuum hose. Imaging was performed on a Phillips CM100 instrument at 100 kV, equipped with a Gatan 1 k CCD camera.

*Reverse-Phase High-Performance Liquid Chromatography (HPLC).* HPLC was utilized to quantify the relative amounts of a dimethacrylate impurity within the HPMA monomer. The experimental setup consisted of an autosampler (Varian model 410), a solvent delivery module

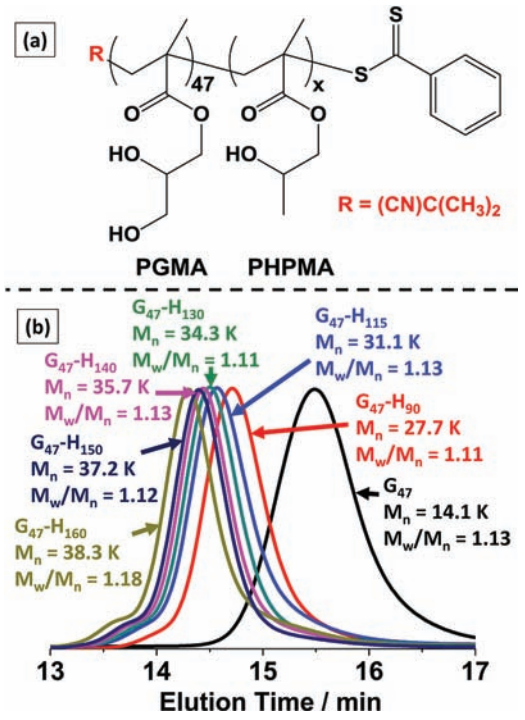


**Figure 1.** (a) Chemical structure of the poly(glycerol monomethacrylate)−poly(2-hydroxypropyl methacrylate) ($PGMA_{47}$-$PHPMA_x$) diblock copolymers synthesized by RAFT aqueous dispersion polymerization at 70 °C. (b) DMF gel permeation chromatograms (vs poly(methyl methacrylate) standards) obtained for a series of six $PGMA_{47}$-$PHPMA_x$ diblock copolymers (and the corresponding $PGMA_{47}$ macro-CTA) synthesized via RAFT aqueous dispersion polymerization at 70 °C and 10 w/v % solids.

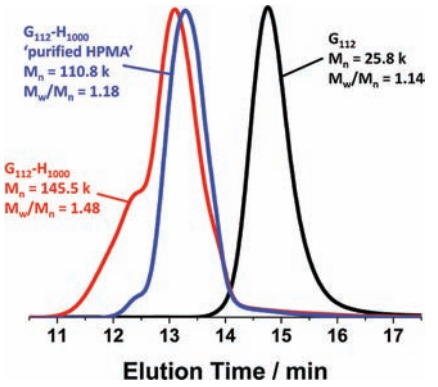


**Figure 2.** DMF gel permeation chromatograms (vs poly(methyl methacrylate) standards) obtained for $G_{112}$-$H_{1000}$ diblock copolymers and the corresponding $G_{112}$ macro-CTA synthesized via RAFT aqueous dispersion polymerization at 70 °C and 10 w/v % solids. The red trace illustrates the influence of small amounts of a dimethacrylate impurity within the HPMA monomer, resulting in light branching and a relatively high polydispersity. However, removal of this dimethacrylate impurity from the HPMA monomer via column chromatography prior to copolymer synthesis leads to a near-monodisperse $G_{112}$-$H_{1000}$ diblock copolymer (blue trace).

(Varian Module 230), a UV detector (Varian model 310), and a Waters SymmetryShield RP18 3.5 $\mu$m, 4.6 × 150 mm HPLC column. The batches of HPMA monomer were allowed to equilibrate at room temperature for 30 min after removing from the freezer prior to opening in order to suppress condensation. Samples were weighed in an autosampler vial and dissolved in acetonitrile to give a concentration of 6.0 mg/mL within 2 h of analysis. The eluent consisted of 0.10% trifluoroacetic acid (TFA) in water and acetonitrile. The following conditions were used: 0−5 min: 70% 0.10% TFA in water. 5−20 min: 70% 0.10% TFA in water to 100% acetonitrile. The UV detector wavelength was 219 nm.

## RESULTS AND DISCUSSION

The initial RAFT polymerization of GMA was conducted in ethanol at 70 °C to generate a hydrophilic, near-monodisperse $PGMA_{47}$ macro-CTA ($M_w/M_n$ = 1.13; Figure 1 and Supporting Information Figure S1). After purification, this macro-CTA was then utilized for the in situ RAFT aqueous dispersion polymerization of HPMA to produce a series of well-defined $G_{47}$-$H_x$ diblock copolymers at 10 w/v % (where G denotes GMA, H denotes HPMA, and $x$ = 90, 115, 130, 140, 150, and 160). $^1$H NMR studies indicated relatively fast polymerization kinetics, with >99% HPMA conversion being achieved within 2 h. Gel permeation chromatography (GPC) studies indicated that near-monodisperse diblock copolymers were obtained with very high blocking efficiencies ($M_w/M_n$ < 1.18) and minimal macro-CTA contamination; see Figure 1b and Supporting Information Figures S2−4). Furthermore, this formulation enables the controlled synthesis of relatively high molecular weight diblock copolymers. For example, $G_{112}$-$H_{1000}$ was readily synthesized with more than 99% HPMA conversion again being obtained within 2 h at 70 °C (see Figure 2 and Supporting Information Figure S4). Good blocking efficiencies were observed, but a rather higher polydispersity was obtained ($M_n$ = 145 500 g mol$^{-1}$, $M_w/M_n$ = 1.48; see Figure 2). This was attributed to small amounts of a dimethacrylate impurity within the HPMA monomer (0.11 mol % as judged by HPLC; see Supporting Information Figure S3), which results in light branching of the PHPMA chains. Silica column chromatography ($CH_2Cl_2$ eluent) was utilized to reduce the dimethacrylate impurity content to below the HPLC detection limit (<0.01 mol %). Using this purified HPMA enabled the synthesis of a near-monodisperse $G_{112}$-$H_{1000}$ diblock copolymer ($M_n$ = 110 800 g mol$^{-1}$, $M_w/M_n$ = 1.18) (see Figure 2).

The $G_{47}$-$H_x$ copolymer particles were analyzed by TEM to assess their morphology (see Figure 3). $G_{47}$-$H_{90}$ generated exclusively spherical micelles (see Figure 3a). Increasing the targeted PHPMA block length leads to a mixture of (mainly) short, linear wormlike micelles and some remaining spherical micelles for $G_{47}H_{115}$ (see Figure 3b). Targeting a block composition of $G_{47}$-$H_{130}$ leads to longer wormlike micelles, with some worms now containing y-junctions or "branch points" (see arrows in Figure 3c and Supporting Information Figure S5). An increase of just 10 HPMA units results in the generation of highly branched, wormlike micelle networks for $G_{47}$-$H_{140}$ (see Figures 3d and Supporting Information Figure S5). $G_{47}$-$H_{150}$ forms an intriguing intermediate phase comprising highly branched wormlike micelles that have partially coalesced to form nascent bilayers (see Figures 3e and Supporting Information Figure S5). Finally, a pure vesicle phase is observed when targeting $G_{47}$-$H_{160}$ (see Figure 3f).

To assess the in situ structural evolution that ultimately leads to vesicle formation by a $G_{47}$-$H_{200}$ copolymer at 10 w/v % and 70 °C, the polymerizing solution was periodically sampled for TEM and $^1$H NMR analysis. The monomer conversion versus time plot provides a fascinating mechanistic insight (see

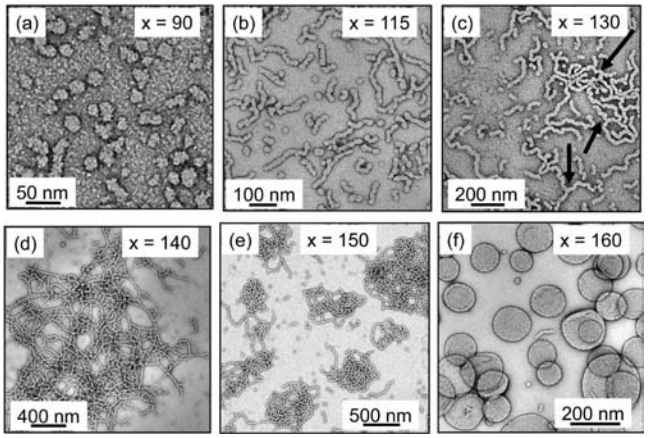


**Figure 3.** Representative TEM images of the final particle morphologies (at >99% conversion and 10 w/v %) observed for a series of six $G_{47}$-$H_x$ diblock copolymers, where $x$ corresponds to (a) 90, (b) 115, (c) 130, (d) 140, (e) 150, and (f) 160. Spherical, worm, and vesicular nanostructures are observed simply by systematically increasing the targeted length of the core-forming PHPMA block.

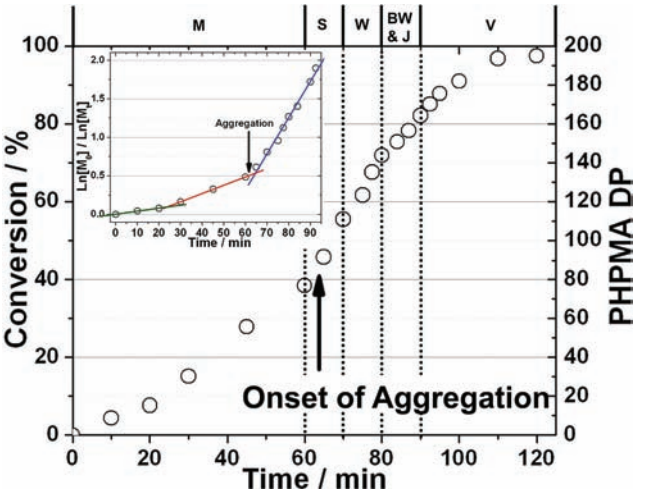


**Figure 4.** HPMA polymerization kinetics obtained for the targeted $G_{47}$-$H_{200}$ diblock copolymer prepared via RAFT aqueous dispersion polymerization at 70 °C and 10 w/v %. The five morphological regimes as judged by TEM are as follows: molecularly dispersed copolymer chains (M), spherical micelles (S), wormlike micelles (W), branched wormlike micelles, jellyfish (BW & J), and vesicles (V). The inset shows a semilogarithmic plot for a subset of these data, which confirms the 5-fold *nucleation-induced* rate enhancement observed on micellar aggregation.

Figure 4). Three distinct regimes are observed. The first regime (green line, see inset) suggests mild retardation, which is commonly observed (but not fully understood) for RAFT polymerization of methacrylates.[34] The second regime is from 20 to 60 min (red line); this corresponds to the formation of molecularly dispersed copolymer chains and involves a modest increase in the slope of the semilogarithmic plot. However, in the third regime, the rate of polymerization increases by a factor of 5 after ~1 h (blue line); this corresponds to the onset of nucleation, since 20 nm micelles are now observed by DLS. This reaction time corresponds to a HPMA conversion of ~45% (i.e., $PHPMA_{90}$), which is consistent with the critical block length previously reported for the micellar aggregation of PHPMA-based diblock copolymers in aqueous solution.[35] We suggest that the unreacted HPMA monomer enters these nascent micelles and solvates the growing PHPMA chains, thus leading to a relatively high local concentration of monomer and hence the observed rate enhancement.

Each aliquot extracted for $^1$H NMR analysis was also analyzed by TEM to assess the evolving *predominant* particle morphologies. As discussed above, no nanostructures were detected within 1 h of the HPMA polymerization. At 65 min (46% conversion, corresponding to $G_{47}$-$H_{92}$), spherical micelles are observed by both DLS and TEM (see Figure 5a). A mixture of spherical micelles and short wormlike micelles is formed after 70 min (55%; $G_{47}$-$H_{110}$). On close inspection of Figure 5b, these short worms are formed by the fusion of spherical micelles into dimers and trimers. Previous studies of the aqueous self-assembly of highly hydrophobic polybutadiene-based amphiphilic block copolymers indicate micellar fusion does not occur on experimental time scales, resulting in a *nonergodic* system with kinetically frozen structures.[17,18] In contrast, micellar fusion has been reported for several systems,[36−38] but only when aided by either cosolvent or added salt. In the present work, the PHPMA chains are relatively solvated by both the HPMA monomer (at intermediate conversions) and water (particularly at shorter PHPMA chain lengths), facilitating the sphere-to-worm transition. This is similar to the recent work of He et al.,[38] who observed micellar fusion at intermediate conversions during the RAFT alcoholic dispersion polymerization of styrene using a poly(acrylic acid) macro-CTA. Based on our own studies, we suggest that the unreacted styrene monomer solvates these growing polystyrene chains, thus facilitating micellar fusion. In order to confirm the swelling of the PHPMA chains by water, a near-monodisperse $PHPMA_{200}$ homopolymer ($M_n$ = 30 000 g mol$^{-1}$, $M_w/M_n$ = 1.13) was synthesized by RAFT in ethanol using the CPDB chain transfer agent. This homopolymer was analyzed by differential scanning calorimetry (DSC) to determine its glass transition temperature ($T_g$). $PHPMA_{200}$ rigorously dried under vacuum at 50 °C for 3 days exhibited a $T_g$ of 95 °C. However, a thin film of $PHPMA_{200}$ that had been soaked in excess water for 10 days prior to DSC studies exhibited a significantly reduced "hydrated $T_g$" of 47 °C due to water uptake. As the reaction temperature (70 °C) is always higher than the "hydrated $T_g$' of the core-forming block (since the PHPMA chains within the cores will have some bound water molecules), this suggests that these growing chains are highly mobile, leading to ergodic aggregates being formed during the polymerization. When the $G_{47}$-$H_{200}$ polymerization is sampled at intermediate conversions, dilution of each extracted aliquot causes any unreacted water-miscible HPMA monomer to immediately diffuse into the aqueous continuous phase, thus quenching the polymerization. Since rapid cooling to 20 °C also occurs during sampling, the intermediate particle morphology is rendered nonergodic (i.e., frozen) and is hence preserved for TEM studies.

Both spherical micelles and linear wormlike micelles are still present after 75 min (62%; $G_{47}$-$H_{123}$; see Figure 5c), but after 78 min (68%; $G_{47}$-$H_{131}$) wormlike micelles constitute the primary morphology. However, at this point, the worms begin to form branch points (primarily y-junctions; see arrows in Figure 5d), due to a reduction in molecular curvature and increased copolymer molecular weight.[17] After 80 min (72%; $G_{47}$-$H_{144}$), the number of worm branch points now increases significantly, with worm clustering observed (see Figures 5e and 6 and Supporting Information Figure S6). Figure 5f and

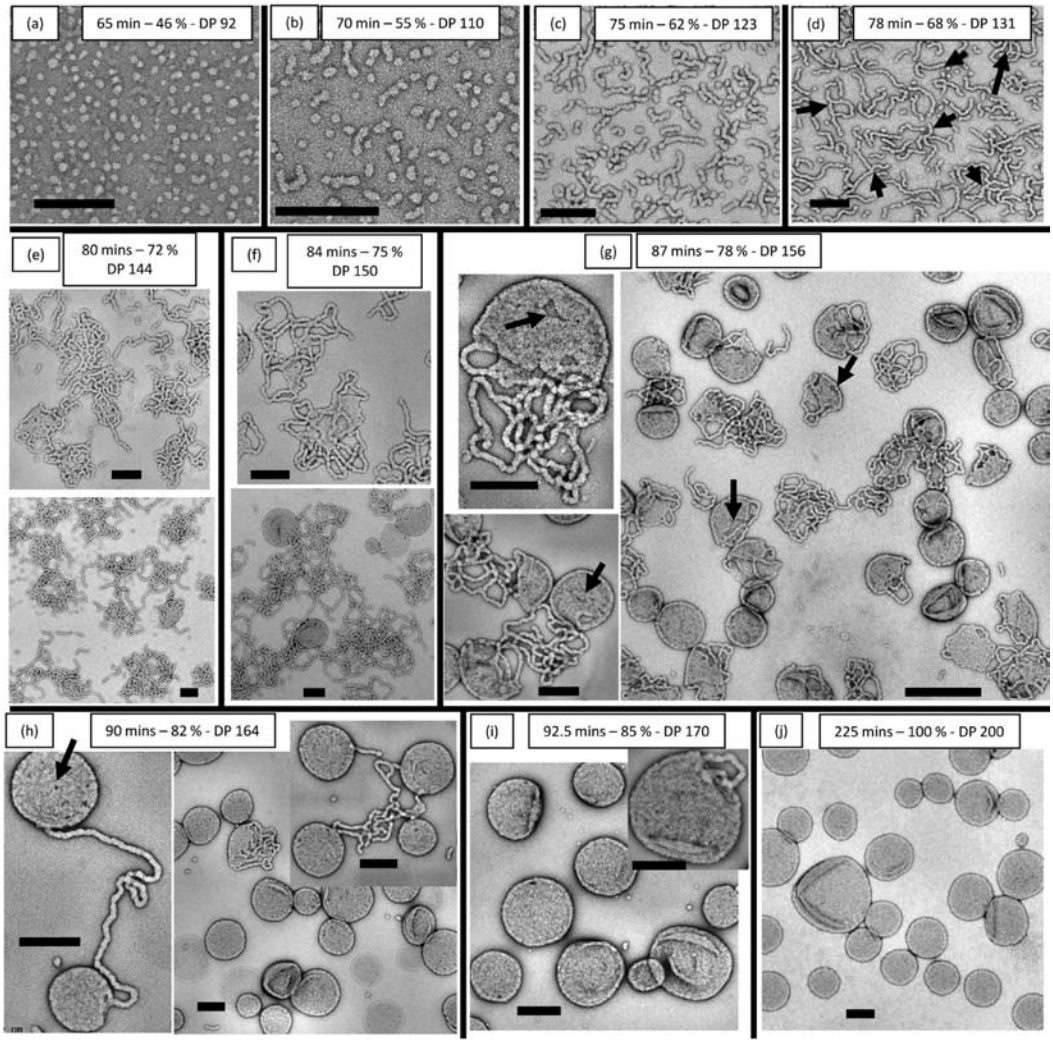


**Figure 5.** Intermediate nanostructures observed during the sphere-to-worm and worm-to-vesicle transitions. Transmission electron micrographs obtained for (a) spheres, (b) short worms, (c) long worms, (d) branched worms, (e,f) partially coalesced worms, (g) jellyfish, and (h−j) vesicles generated in situ after various reaction times for a target $G_{47}$-$H_{200}$ diblock copolymer prepared by RAFT aqueous dispersion polymerization at 70 °C and 10 w/v % solids. Scale bars = 200 nm.

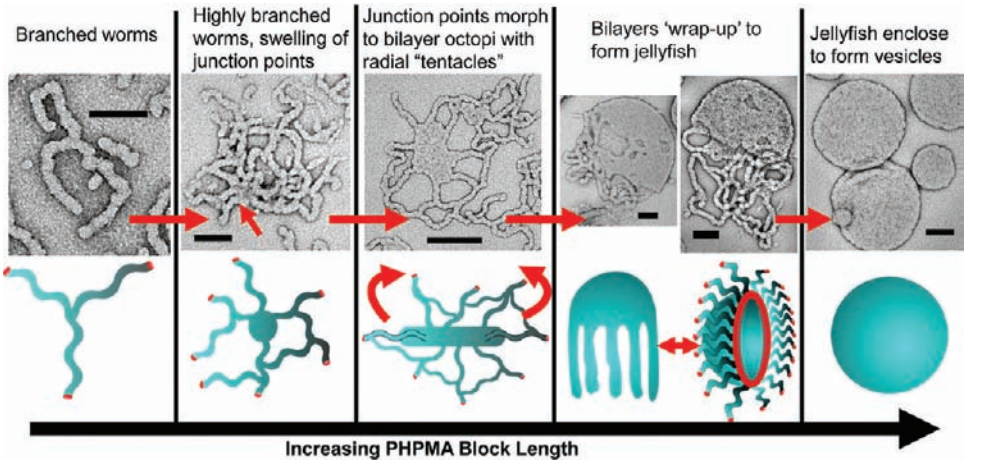


**Figure 6.** Suggested mechanism for the polymerization-induced worm-to-vesicle transformation during the synthesis of $G_{47}$-$H_{200}$ by RAFT aqueous dispersion polymerization.


dx.doi.org/10.1021/ja206301a |*J. Am. Chem. Soc.* 2011, 133, 16581–16587

Supporting Information Figure S6 show how these highly branched structures undergo partial coalescence and develop nascent bilayers with protruding "tentacles" (84 min; 75%; $G_{47}$-$H_{150}$). This octopus-like morphology has been previously reported for a *binary mixture* of two poly(ethylene oxide)−polybutadiene diblock copolymers.[17] The present work suggests that this is an *intrinsic* intermediate morphology between worms and bilayers formed by polymerization-induced self-assembly of a *single* copolymer. After 87 min (78%; $G_{47}$-$H_{156}$), these octopi structures then undergo partial wrap-up and form "jellyfish" (see Figures 5g and 6 and Supporting Information Figure S6) with surface pores and defects due to incomplete worm/bilayer fusion (see arrows in Figure 5g and h). In essence, the hemispherical jellyfish structures appear to be the final stage prior to vesicle formation. The jellyfish "tentacles" undergo fusion after 90 min (82%; $G_{47}$-$H_{164}$). This produces a predominantly vesicular phase, but some vesicles do remain interconnected via residual "tentacles" (see Figure 5h and i). However, as the surface pores coalesce at higher HPMA conversions, *defect-free* vesicles are first observed after 100 min (91%; $G_{47}$-$H_{182}$) (see Supporting Information Figure S6f) and finally a pure vesicle phase is formed after 225 min (>99%; $G_{47}$-$H_{200}$) (see Figures 5j and 6).

The above observations are consistent with previous studies of the worm-to-vesicle transition that occurs on rapidly diluting polystyrene−poly(acrylic acid) diblock copolymers in dioxane/water mixtures with further water.[39] A two-step transition was reported, in which the rods/worms first flatten to form lamellae, followed by wrap-up of the lamellae to produce vesicles. However, the additional intermediate morphologies observed in the present work, which are only observed over a narrow range of diblock compositions, significantly enhance our understanding of the detailed mechanism of vesicle formation.

For the structural evolution during the synthesis of $G_{47}$-$H_{200}$, the in situ morphologies obtained at a given time (and hence mean DP for the growing PHPMA block) correspond closely to the final post mortem morphologies observed at full conversion when targeting the equivalent DP. For example, spherical micelles are obtained when targeting $G_{47}$-$H_{90}$ (see Figure 3a), which is the same morphology as that observed after 65 min (or 46% conversion, corresponding to an in situ block composition of $G_{47}$-$H_{92}$; see Figure 5a) during the polymerization of $G_{47}$-$H_{200}$. Similarly, close correspondence between the in situ block compositions and the final post mortem compositions is also observed for the wormlike micelles and vesicles (compare Figures 3 and 5). This is an important insight, because it suggests that the unreacted HPMA monomer does not affect the intermediate morphologies that are observed during the kinetic studies when targeting a final block composition/morphology of $G_{47}$-$H_{200}$ vesicles.

Our aqueous dispersion polymerization formulation offers a number of advantages for polymerization-induced self-assembly compared to aqueous emulsion[40−43] or alcoholic dispersion[38,44−46] polymerization formulations reported in the literature. In the former case, the worm or vesicle phases are typically contaminated with spheres and, although monomer conversions are usually high, they do not exceed 95%. Moreover, relatively high copolymer polydispersities are often observed,[40−42] although a new report describes rather better results for such emulsion polymerization syntheses.[43] In the latter case, Pan and co-workers[38,44−46] have reported low polydispersities ($M_w/M_n$ < 1.20) for the polymerization of styrene in methanol and relatively pure phases can be obtained (i.e., solely spheres, worms or vesicles), but relatively low styrene conversions (typically < 70%) are obtained. The gradual evolution of spheres to worms to vesicles was observed in this earlier study, *but none of the complex intermediate morphologies observed herein (partially coalesced nascent bilayers, jellyfish, etc.) that are essential for a more complete mechanistic understanding have been previously reported.*[38,45,46] We believe that these new insights have been achieved by extensive sampling of the in situ HPMA polymerization, although it is also possible that there are intrinsic differences between RAFT aqueous dispersion polymerization and RAFT syntheses conducted under either aqueous emulsion or alcoholic dispersion polymerization conditions.

## CONCLUSIONS

In summary, polymerization-induced self-assembly via RAFT aqueous dispersion polymerization of HPMA using a PGMA macro-CTA leads to near-monodisperse diblock copolymers, which form spheres, worms, and vesicles, depending on the targeted block composition. The onset of micellar nucleation corresponds to an enhancement in the rate of polymerization (>99% HPMA monomer conversion within 2 h), which suggests solvation of the growing PHPMA chains by the unreacted HPMA monomer. Moreover, close monitoring of the in situ HPMA polymerization by TEM reveals a range of *intermediate* morphologies, which provide important mechanistic insights regarding the sphere-to-worm and worm-to-vesicle transitions.

## ASSOCIATED CONTENT

**Supporting Information.** Details of the HPMA monomer purification, further details of the synthesis of high molecular weight $G_{112}$-$H_{1000}$ copolymers, and additional TEM images. This material is available free of charge via the Internet at http://pubs.acs.org

## AUTHOR INFORMATION

**Corresponding Author**
s.p.armes@sheffield.ac.uk

## ACKNOWLEDGMENT

A.B. thanks the EPSRC (EP/E012949/1) for postdoctoral funding. Dr. Svetomir Tzokov is thanked for preparing the carbon-coated TEM grids.

## REFERENCES

(1) Alberts, B.; Johnson, A.; Lewis, J.; Raff, M.; Roberts, K.; Walter, P. *Molecular Biology of the Cell*, 4th ed.; Garland Science: New York, 2002.
(2) Balmbra, R. R.; Clunie, J. S.; Goodman, J. F. *Nature* **1969**, *222*, 1159–1160.
(3) Israelachvili, J. N. *Intermolecular & Surface Forces*, 2nd ed.; Academic Press: London, 1991; Vol. 1.
(4) Israelachvili, J. N.; Mitchell, D. J.; Ninham, B. W. *J. Chem. Soc., Faraday Trans.* **1976**, *72*, 1525–1568.
(5) Zhang, L. F.; Eisenberg, A. *Science* **1995**, *268*, 1728–1731.
(6) Won, Y. Y.; Davis, H. T.; Bates, F. S. *Science* **1999**, *283*, 960–963.
(7) Li, Z. B.; Kesselman, E.; Talmon, Y.; Hillmyer, M. A.; Lodge, T. P. *Science* **2004**, *306*, 98–101.
(8) Cui, H. G.; Chen, Z. Y.; Zhong, S.; Wooley, K. L.; Pochan, D. J. *Science* **2007**, *317*, 647–650.
(9) Wang, X. S.; Guerin, G.; Wang, H.; Wang, Y. S.; Manners, I.; Winnik, M. A. *Science* **2007**, *317*, 644–647.

(10) Pochan, D. J.; Chen, Z. Y.; Cui, H. G.; Hales, K.; Qi, K.; Wooley, K. L. *Science* **2004**, *306*, 94–97.
(11) Jain, S.; Bates, F. S. *Science* **2003**, *300*, 460–464.
(12) Discher, D. E.; Eisenberg, A. *Science* **2002**, *297*, 967–973.
(13) Christian, D. A.; Tian, A. W.; Ellenbroek, W. G.; Levental, I.; Rajagopal, K.; Janmey, P. A.; Liu, A. J.; Baumgart, T.; Discher, D. E. *Nat. Mater.* **2009**, *8*, 843–849.
(14) Massignani, M.; LoPresti, C.; Blanazs, A.; Madsen, J.; Armes, S. P.; Lewis, A. L.; Battaglia, G. *Small* **2009**, *5*, 2424–2432.
(15) Howse, J. R.; Jones, R. A. L.; Battaglia, G.; Ducker, R. E.; Leggett, G. J.; Ryan, A. J. *Nat. Mater.* **2009**, *8*, 507–511.
(16) Blanazs, A.; Armes, S. P.; Ryan, A. J. *Macromol. Rapid Commun.* **2009**, *30*, 267–277.
(17) Jain, S.; Bates, F. S. *Macromolecules* **2004**, *37*, 1511–1523.
(18) Fernyhough, C.; Ryan, A. J.; Battaglia, G. *Soft Matter* **2009**, *5*, 1674–1682.
(19) Discher, B. M.; Won, Y. Y.; Ege, D. S.; Lee, J. C. M.; Bates, F. S.; Discher, D. E.; Hammer, D. A. *Science* **1999**, *284*, 1143–1146.
(20) Bermudez, H.; Brannan, A. K.; Hammer, D. A.; Bates, F. S.; Discher, D. E. *Macromolecules* **2002**, *35*, 8203–8208.
(21) Battaglia, G.; Ryan, A. J. *J. Am. Chem. Soc.* **2005**, *127*, 8757–8764.
(22) Du, J. Z.; Tang, Y. P.; Lewis, A. L.; Armes, S. P. *J. Am. Chem. Soc.* **2005**, *127*, 17982–17983.
(23) Blanazs, A.; Massignani, M.; Battaglia, G.; Armes, S. P.; Ryan, A. J. *Adv. Funct. Mater.* **2009**, *19*, 2906–2914.
(24) Napoli, A.; Valentini, M.; Tirelli, N.; Muller, M.; Hubbell, J. A. *Nat. Mater.* **2004**, *3*, 183–189.
(25) Qin, S. H.; Geng, Y.; Discher, D. E.; Yang, S. *Adv. Mater.* **2006**, *18*, 2905.
(26) LoPresti, C.; Lomas, H.; Massignani, M.; Smart, T.; Battaglia, G. *J. Mater. Chem.* **2009**, *19*, 3576–3590.
(27) Hayward, R. C.; Pochan, D. J. *Macromolecules* **2010**, *43*, 3577–3584.
(28) Lipic, P. M.; Bates, F. S.; Hillmyer, M. A. *J. Am. Chem. Soc.* **1998**, *120*, 8963–8970.
(29) Hamley, I. W.; Stanford, J. L.; Wilkinson, A. N.; Elwell, M. J.; Ryan, A. J. *Polymer* **2000**, *41*, 2569–2576.
(30) An, Z. S.; Shi, Q. H.; Tang, W.; Tsung, C. K.; Hawker, C. J.; Stucky, G. D. *J. Am. Chem. Soc.* **2007**, *129*, 14493–14499.
(31) Delaittre, G.; Save, M.; Charleux, B. *Macromol. Rapid Commun.* **2007**, *28*, 1528–1533.
(32) Rieger, J.; Grazon, C.; Charleux, B.; Alaimo, D.; Jérôme, C. *J. Polym. Sci., Part A: Polym. Chem.* **2009**, *47*, 2373–2390.
(33) Li, Y.; Armes, S. P. *Angew. Chem., Int. Ed.* **2010**, *49*, 4042–4046.
(34) Moad, G.; Rizzardo, E.; Thang, S. H. *Acc. Chem. Res.* **2008**, *41*, 1133–1142.
(35) Madsen, J.; Armes, S. P.; Bertal, K.; MacNeil, S.; Lewis, A. L. *Biomacromolecules* **2009**, *10*, 1875–1887.
(36) Denkova, A. G.; Mendes, E.; Coppens, M. O. *J. Phys. Chem. B* **2009**, *113*, 989–996.
(37) Burke, S. E.; Eisenberg, A. *Langmuir* **2001**, *17*, 6705–6714.
(38) He, W.-D.; Sun, X.-L.; Wan, W.-M.; Pan, C.-Y. *Macromolecules* **2011**, *44*, 3358–3365.
(39) Chen, L.; Shen, H. W.; Eisenberg, A. *J. Phys. Chem. B* **1999**, *103*, 9488–9497.
(40) Delaittre, G.; Dire, C.; Rieger, J.; Putaux, J.-L.; Charleux, B. *Chem. Commun.* **2009**, 2887–2889.
(41) Rieger, J.; Zhang, W. J.; Stoffelbach, F.; Charleux, B. *Macromolecules* **2010**, *43*, 6302–6310.
(42) Boisse, S.; Rieger, J.; Belal, K.; Di-Cicco, A.; Beaunier, P.; Li, M. H.; Charleux, B. *Chem. Commun.* **2010**, *46*, 1950–1952.
(43) Zhang, X.; Boissé, S.; Zhang, W.; Beaunier, P.; D'Agosto, F.; Rieger, J.; Charleux, B. *Macromolecules* **2011**, *44*, 4149–4158.
(44) Huang, C.-Q.; Pan, C.-Y. *Polymer* **2010**, *51*, 5115–5121.
(45) Cai, W.-M.; Wan, W.-M.; Hong, C.-Y.; Huang, C.-Q.; Pan, C.-Y. *Soft Matter* **2010**, *6*, 5554–5561.
(46) Wan, W.-M.; Pan, C.-Y. *Polym. Chem.* **2010**, *1*, 1475–1484.